10. S. P. Lin, Progr. Heat & Mass Transfer, Proc. Int. Symp. Two-Phase Syst., Haifa, 1971, Vol. 6, 263-275, Oxford (1972).
11. Yu. A. Buevich, Inzh.-Fiz. Zh., 48, No. 2, 230-239 (1985).
12. H. Linde, P. Schwartz, and H. Wilke, Hydrodynamics of Interphasal Surfaces [in Russian], Moscow (1984), pp. 76-116.
13. A. Sanfeld, A. Steinchen, M. Hannenberg, et al., Hydrodynamics of Interphasal Surfaces [in Russian], Moscow (1984), pp. 45-78.
14. Yu. A. Buevich and S. V. Kudymov, Inzh.-Fiz. Zh., 45, No. 4, 566-576 (1983).

STABILITY CRITERION OF THREE-DIMENSIONAL PERTURBATIONS ON CONCAVE ELASTIC SURFACES

N. F. Yurchenko and V. V. Babenko

UDC 532.526

Stability criteria are determined experimentally for the boundary layer on concave elastic surfaces in the preturbulent transition region.

As always, the investigation of the physical processes of turbulent boundary-layer formation remains urgent for a broad class of scientific and practical problems. The structure of the perturbing motion in different stages of laminary boundary-layer transition into turbulent and the process of transformation of plane into three-dimensional perturbations are studied experimentally in [1], in longitudinal vortices of the Benny–Lin type on a flat plate, and in Goertler vortices on a curvilinear plate. The general features and regularities of formation and existence of these vortical systems are determined and the Goertler neutral curve is first constructed by experimental means.

The possibility of controlling the hydrodynamic stability by using different elastic plates is studied in [2], and three-dimensional perturbations on a rigid plate in [3].

The purpose of the present paper is to investigate the influence of an elastic surface on the stability of longitudinal vortices and to determine the possibility of controlling three-dimensional perturbations, particularly, for heat- and mass-transfer problems.

The methodology of the experiment is based on the susceptibility of the boundary layer to different perturbations [1, 4, 5]. According to these representations, under ideal flow conditions prerequisites exist for the generation of perturbations in the form of Tollmien–Schlichting waves with their subsequent transformation into more complex types. Factors degrading the hydrodynamic stability (for instance, the high degree of main flow turbulence, streamlined surface roughness, etc.) result in magnification of the perturbing motions. The greater the intensity and quantity of the degrading factors, the more rapidly do natural boundary layer perturbations develop. The susceptibility problem consists of studying the nature of the interaction at different stages of boundary layer transition between existing natural perturbations and those induced from outside.

On the basis of this definition the linear and Goertler instabilities are particular cases of the susceptibility problem whose investigation must be conducted under the greatest possible ideal fluid flow conditions and the induction of small perturbations. On the one hand, by this the influence of uncontrollable factors and nonlinear interaction of the induced and natural perturbations on stability is eliminated, and on the other, the possibility is achieved of determining the boundary-layer reaction to perturbations of a given scale. The induced small plane perturbations magnify and interact with the natural perturbations in the linear stability investigation. Small three-dimensional perturbations, which excite the existing plane natural perturbations and result in their rapid transformation into three-dimensional perturbations that interact with the induced perturbations are introduced into the boundary layer in the study of the Goertler instability.

Institute of Hydromechanics, Academy of Sciences of the Ukrainian SSR, Kiev. Translated from Inzhenerno-Fizicheskii Zhurnal, Vol. 52, No. 5, pp. 781-787, May, 1987. Original article submitted December 30, 1986.

 0022-0841/87/5205-0568$12.50

The experiment was conducted on a hydrodynamic test stand with a regulatable turbulence level $\varepsilon \approx (0.05\text{-}10)\%$ [1, 2]. The boundary layer was investigated on the bottom of the working section which was in the form of four variants: flat along the whole length of 3 m, and with a concave part of curvature $1/R = 1$, 0.25, and 0.08 m^{-1}, where R is the radius of curvature.

In all cases the distance between the leading edge and the beginning of the curvature was 0.5 m and the maximal deflection was 0.05 m. The nonuniformity in the velocity distribution along the working section axis reached 20%. A transparent curvilinear cover was fabricated that duplicated the configuration of the bottom with $1/R = 1\ m^{-1}$. Installation of the cover above this bottom permitted flow realization in a cylindrical channel. Therefore, the regularities of vortex perturbation development could be investigated in both a classical formulation (in the channel), and under complicating conditions (without the cover): raising the degree of turbulence and the variable longitudinal pressure gradient.

As in [6], the longitudinal vortex perturbations were introduced by using vortex generators installed in the transversal direction (z) on the streamlined surface. The vortex generator is a vertical plate $5\cdot10^{-5}$ m thick with a bifurcated and slightly cambered endface such that vane surfaces to twist the flow were on both sides of the plate. This resulted in the formation of pairs of longitudinal vortices between adjacent vortex generators: the slow flow domain ("peak" $z = 0$) was formed in the xz plane in the wake behind the vortex generator, and the accelerated flow domain ("valley", $z = \lambda_z/2$). The distance λ_z between vortex generators corresponded to the wavelength of the three-dimensional perturbations and varied between 0.004-0.032 m limits with a 0.002-m step. Four kinds of vortex generators of similar shape, fabricated by one die, were utilized. They differed in length and height: the vortex generators B1 were 0.003 m high and 0.012 m long, B2 were, respectively 0.005 and 0.015 m, B3 were 0.007 and 0.018 m, B4 were 0.015 and 0.018 m.

The perturbation development was observed by using flow visualization by a tellurium method during boundary-layer parameter checking by a laser anemometer [1-6]. The regularities of three-dimensional perturbations in the form of longitudinal vortices were investigated by placing cascades of vortex generators at different places along the x axis of the working section and downstream at a distance of $x_- = 5\cdot10^{-2}$ m from them by a hot wire to photograph the visualized velocity profile in the transversal direction. Vortex generators were inserted in the boundary layer at $x = \text{const}$, their size and the wavelength λ_z were varied by changing the distance between them as well as the quantity U_∞. The profile U(z) was photographed at different distances y from the wall. To refine the details at characteristic places in z, the streamlines and U(y) profiles which were also checked by using the laser anemometer, were photographed.

By measuring the parameters and regularities of vortex system development along x for U_∞, R and $\lambda_z = \text{constant}$, we determine the displacement of the control point on the Goertler stability graph along the line $P = U_\infty \lambda_z^{1,5} \nu^{-1} R^{-0,5} = \text{const}$ (P is the wave parameter, and ν is the kinematic viscosity coefficient). By alternately varying the values of R, U_∞ and λ_z, we pass along different lines $P = \text{const}$. The right branch of the Goertler neutral curve and the domain of maximal amplifications of the vortex systems were here determined. The intersection of the neutral curve is characterized by the formation of the most stable waveform profile U(z) in space and time.

If λ_z changes for R, U_∞ and $x = \text{const}$, then the control point on the graph of the Goertler curve advanced along the line $G = U_\infty \delta_2^{1,5} \nu^{-1} \times R^{-0,5} = \text{const}$, where G is the Goertler parameter and δ_2 is the thickness of the loss of momentum. Varying the values of R and U_∞ alternately, we pass along different lines G. Therefore, it is possible to determine a lower minimal value of G and the left branch of the neutral curve.

Finally, by comparing the results of measurements for λ_z, U_∞ and $x = \text{const}$ for different R, we move the control point along the lines $\alpha_z \delta_2 = \text{const}$, where $\alpha_z = 2\pi/\lambda_z$ is the wave number.

For the same x and U_∞ the U(z) profiles were initially investigated for the natural transition. In addition to these, the measurements on the rigid curvilinear plates were controls for the studied longitudinal vortex systems [1]. These plates were then glued to a monolithic elastic material of thickness 0.003 m and density 120 kg/m^3. The mechanical properties of the elastomer were characterized by the instantaneous elastic modulus $E = 5\cdot10^5$ N/m^2 and the loss angle tangent $\tan \varphi = 0.62$.

Graphical copies of the photographs of the flow field along the curvilinear elastic

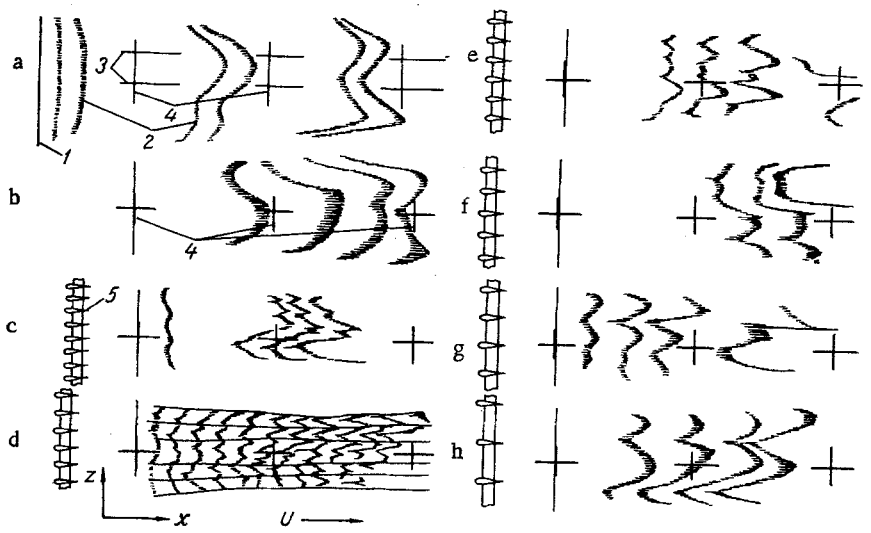

Fig. 1. Boundary-layer reaction of an elastic surface to perturbations of different scale: R = 4 m, U_∞ = 0.033 m/sec, x = 2.2 m; x_- = 0.05 m; $y_{t.w.}$ = 0.006 m; without induction of perturbation on the rigid (a) and elastic (b) surfaces; c — h with the induction of perturbation for λ_z=0,01 м (c); 0.012 m (d); 0.014 m (e); 0.016 m (f); 0.02 m (g); 0.028 m (h): 1) tellurium wine; 2) tellurium cloud; 3) longitudinal and 4) transverse markers on the bottom of the working section; 5) vortex generators; spacing 0.5 m between transverse, and 0.1 m between longitudinal markers.

surface visualized in the xz plane are represented in Fig. 1. The flow field (the location of the tellurium wire 1) was recorded at a distance from the streamlined surface that was approximately equal to the displacement thickness δ_1 ($y_{t.w.} \approx 0{,}006$ m) . Tellurium clouds were emitted automatically during the supply of electrical pulses to the wire at regulated time intervals (0.5 sec). During propagation downstream the linear cloud was initially deformed in conformity with the velocity field in the boundary layer, i.e., acquired the form of the U(z) profile. The decimeter markers 3 and 4 superposed on the surface along the channel axis permitted computation of the propagation velocity and the perturbation growth along x as a function of the coordinate z. The different shape of the tellurium clouds emitted as successive times characterized the nonstationarity of the flow field above the concave elastic surface. As compared with the rigid standar, the natural perturbations on the elastic surface differed by their larger scale and lower rates of growth downstream.

Installation of the cascade of vortex generators 5 (Fig. 1c-h) modified the flow pattern substantially. For a small value of λ_z (c) the imposition of a fine-scaled induced structure on the large-scale is natural. In contrast to the concave rigid surface, such an effect here appeared downstream from the vortex generator cascade (compare with [1]). Superposition of the induced and natural perturbations was detected in the flow around the plane rigid plate when perturbations of lower intensity were introduced. The effect described shows that the growth rate for the natural perturbations is greater than for those induced with a low value of λ_z: modulation of the natural wave was observed prior to the start of "longitudinal braid formation" with stimulated λ_z. Therefore, organization of the given flow structure in the boundary layer of curved monolithic elastic surfaces requires the insertion of sufficiently intensive perturbations on the one hand, and on the other, such a structure is formed at a great distance downstream from the site of occurrence. In other words, the boundary layer on elastic surfaces is a more inertial system than on rigid surfaces. The data obtained are in good agreement with the deductions of [5], according to which a more intensive formation of Benny—Lin vortices occurred as compared with the rigid etalon in a natural transition to elastic horizontal uniform plates, as did their slow development downstream, while the interaction with the imposed field of three-dimensional perturbations depended on the scale relationships between the natural and induced perturbations and contributed to protracting the transition.

The smoothing, damping nature of the influence of the elastic surfaces on the development

TABLE 1. Perturbed Boundary-Layer Parameters in a Cylindrical Section

x, m	U_∞, m/sec	$\delta \cdot 10^3$, m	$\delta_1 \cdot 10^3$, m	$\lambda_z \cdot 10^2$, m	$x_- \cdot 10^2$, m	$(\delta_-) \cdot 10^3$, m	$(\delta_1) \times 10^3$, m	$(\delta_2) \times 10^3$, m	G	$\alpha_z \delta_2$
0,85	0,107	15	1,9	2	5	20	3	1,67	7,2	0,52
0,9	0,2	13	1,67	2	5	19	2,45	1,94	18,8	0,61
0,85	0,106	15	1,9	2	10	15	2,9	1,71	7,5	0,52
0,85	0,105	15	1,9	2,8	5	20	2,2	1,5	6,1	0,34
0,9	0,055	20	4 43	2,4	5	20	5,1	2,76	80	0,72

of processes in the boundary layer made difficult finding clear boundaries of the three-dimensional perturbation growth and damping domains. In this case the principle of boundary layer selectivity reaction with respect to the scale λ_z of the induced perturbations is not manifest so clearly and does not afford a possibility of determining the neutral perturbations uniquely as occurred for the rigid surface [1]. From an analysis of the data (Fig. 1d-g) it follows from the criteria taken for the stiff wall the structures with $\lambda_z = 0.012$-0.02 m might equally be such perturbations. Computation of the parameters to construct the stability diagram yields the following quantities here: $G = 2.1$ $\alpha_z \delta_2 = 0.5$-0.84. The induced perturbations with $\lambda_z = 0.028$ m that are being magnified (Fig. 1h) are characterized by the parameters $G = 2.1$ and $\alpha_z \delta_2 = 0.36$ and the natural perturbations with $\lambda_z = 0.05$ m by the quantities $G = 2.1$ and $\alpha_z \delta_2 = 0.2$. Let us note that the natural perturbations are stabilized best by those imposed with $\lambda_z = 0.012$ (Fig. 1d).

The cycle of investigations on the same elastic surface in a cylindrical section yielded several points of the stability diagram. Results of not only the U(z) profile visualization but also measurements of the U(y) profile by the laser anemometer were utilized. Only those U(y) profiles were analyzed for three coordinates z (at the "peaks," "valleys," and intermediate positions) which had the characteristic form for the developed longitudinal vortex system (respectively with an inflection point at the wall, filled without points of inflection, and an abrupt inflection in the neighborhood $y \approx \delta_1$ [6]). The parameters G and $\alpha_z \delta_2$, obtained for such conditions can, as the last pair for the concave wall, be referred to the maximal magnification domain on the stability diagram. Presented in the table are kinematic boundary layer characteristics in the cylindrical section in the presence of such perturbations. The pairs of parameters obtained are superposed in the form of points on the Goertler stability diagram network (Fig. 2). Despite the fact that no clear boundary is determined between the damping and growing perturbations (neutral curve), it can be asserted that a smaller perturbation range is enclosed by the instability domain here than in the case of a rigid surface.

Another important result is the increase in the first and second critical Goertler numbers. The first critical Goertler number G_0 is the minimal value of the quantity G for which the neutral development of longitudinal vortices is fixed; it characterizes the beginning of the formation of ordered longitudinal vortex systems in the boundary layer and is determined by the minimal extremal point of the Goertler neutral curve. Results of investigating the linear boundary layer stability [1, 2] indicate an increase in G_0 for elastic plates as compared with a rigid plate for which $G_0 = 0.3$-0.5 [1]. According to the data in Fig. 2, for elastic plates G_0 increased 2-3 times.

The second critical Goertler number characterizes destruction of the ordered vortex systems and transition to turbulence. Depending on the flow conditions, $G_* = 2$-8 and 1-1.5 are obtained in [8, 9], respectively, for a rigid plate, and oscillations of the longitudinal vortices in z (meandering) for $G = 6$-7 are fixed in [8]. The quantities $G_* = 18.8$ are obtained in the present measurements for the artificial generation of vortex perturbations above an elastic surface for an open channel with a concave section and $G_* = 80$ for a cylindrical channel. For the rigid concave wall $G_* = 6.3$ [1], i.e., is 3-12 times less than for an elastic surface are also taken into account, then evidently the nonlinear transition domain is here increased.

Therefore, as for the flow around a flat plate [1, 5], the results obtained showed that the curvilinear elastic surface also effectively stabilizes three-dimensional perturbations, the extent of the stable longitudinal vortex systems increases substantially here as compared with the rigid plate. The longitudinal vortex systems on a rigid plate were controlled in [3] by using distributed vortex generators which were heated to increase the efficiency.

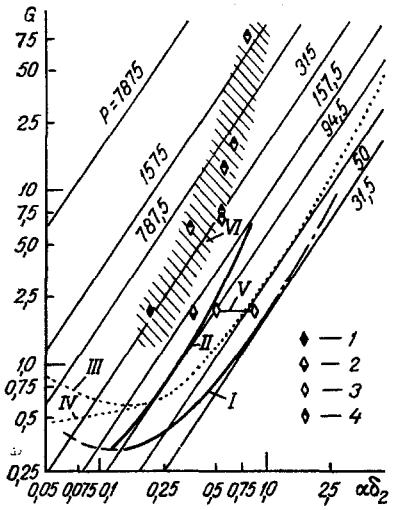

Fig. 2. Stability of three-dimensional perturbations on a concave elastic surface: I, II) experimental neutral curve and maximal magnification curve for a rigid surface [1]; III, IV) computed neutral curves [7]; V, VI) domains of neutral and maximally growing perturbations for an elastic surface; characteristics of a concave elastic surface: 1) natural perturbations; 2) growing forced; 3) almost neutral forces; 4) growing forced in a cylindrical channel.

The present tests show that either uniform elastic surfaces or those ordered in the transversal direction [10] can be used here successfully for these purposes since the property of such plates to organize and stabilize the longitudinal vortex system was detected here.

It is known that the heat and mass transfer processes are intensified in vortical motion. As is shown [1], longitudinal vortex systems are characterized simultaneously by minimal friction drag coefficient. Then application of elastic ordered surfaces permits increasing the intensity of the heat and mass transfer in the near-wall domain with a simultaneous stable reduction in the friction coefficient. Conservation of the fundamental modeling principles is required here. On the basis of making the coefficients of the differential equations of elastic surface motion dimensionless in the form of the Voight–Kelvin model [2, 10], dimensionless parameters characterizing the properties of the elastic materials utilized were compiled and computed. The inertial properties were determined by the coefficient of fluctuating mass $M=\rho l/\rho_0\delta_1$, $M^*=\rho l/\rho_0\bar{\delta}_1$, where δ_1 and $\bar{\delta}_1$ are the boundary layer displacement thicknesses for its natural development and for the introduction of controlled perturbations. The elastic and damping properties were characterized by the Cauchy C and damping D parameters:

$$C=\rho_0U_\infty^2/2E, \qquad D=k\rho_0U_\infty^2/2\sqrt{\overline{(p')^2}}.$$

Here k is proportional to the energy being absorbed by the layer of elastic material ($k=1-\exp[-\pi\,\mathrm{tg}\,\varphi]$) . For the material used in the present experiments the magnitudes of the similarity criteria had the values M = 0.2, M* = 0.16; C = $1.25\cdot10^{-4}$ and D = 98.8. For other materials tested these quantities varied between the limits M = 0.09–0.89, M* = 0.16–0.54, C = $(0.4\text{–}2.4)\cdot10^{-4}$, and D = 72.9–98.8. It was also determined that intensification of the heat and mass transfer processes for the generation of vortex system in the boundary layer can be achieved on a plate being characterized by the set of parameters M = 0.7, M* = 0.66, C = $0.5\cdot10^{-4}$, and D = 73.3. Geometric similarity in the transverse regularity step λ_z of the induced longitudinal vortex system should here also be taken into account and in the case of an elastic surface with an ordered outer layer in the transversal direction, the step in this

ordering as well. To produce and maintain longitudinal vortes structures contributing to the best mixing of a medium near a streamlined surface, the selection of the step in λ_z should be performed on the basis of a conversion of the perturbation parameters incident in the neutral stability domain (Fig. 2). In this case the blurred nature of this domain (in contrast to the localized curve for a rigid surface) plays an affirmative part by giving a certain range of acceptable values of λ_z. In its turn, this increases the possibility of selecting the perturbation scale needed without damping and without resulting in rapid turbulization of the boundary layer.

NOTATION

x, y, z, coordinate axes governing the flow field and directed, respectively, along the main flow, perpendicular to the wall, and across the flow; R, surface radius of curvature; U_∞, unperterbed flow velocity; Re, Reynolds number defined with respect to the length; P, Goertler wave parameter; G_0 and G_*, respectively, the first and second critical Goertler numbers; p', magnitude of the pressure fluctuations in the boundary layer; M, C, D, parameters characterizing the inertial, elastic, and damping properties, respectively, of the materials; l, the thickness of the elastic material layer; E, elastic modulus; k, damping factor; tan φ, loss angle tangent; ρ and ρ_0, magnitudes of the streamlining medium and the elastic material; δ_1, boundary-layer displacement thickness; δ_2, loss of momentum thickness; $\alpha_z = 2\pi/\lambda_z$ and λ_z, wave number and wavelength of the three-dimensional perturbations along z; ε, degree of turbulence; x_-, distance between the vortex generator and the tellurium wire; and ν, kinematic viscosity coefficient.

LITERATURE CITED

1. L. F. Kozlov, A. I. Tsyganyuk, V. V. Babenko, et al., Turbulence Formation in Shear Flows [in Russian], Kiev (1985).
2. L. F. Kozlov and V. V. Babenko, Experimental Boundary-Layer Investigations [in Russian], Kiev (1978).
3. N. F. Yurchenko, V. V. Babenko, and L. F. Kozlov, Lmanar-Turbulent Transition. IUTAM Symp. Novosibirsk, 1984, 329-335, Springer-Verlag, Berling, Heidelberg (1985).
4. V. V. Babenko, V. P. Ivanov, and N. F. Yurchenko, Avtometriya, No. 3, 91-96 (1982).
5. L. F. Kozlov, V. V. Babenko, N. F. Yurchenko, and V. P. Ivanov, Near-Wall Turbulent Flows, 95-105, Novosibirsk (1984).
6. N. F. Yurchenko, Inzh.-Fiz. Zh., 41, No. 6, 966-1002 (1981).
7. A. M. O. Smith, Q. Appl. Math., 13, 233-262 (1955).
8. S. H. Winoto, D. F. G. Durao, and B. I. Grane, Trans. ASME, J. Fluid Eng., 101, 517-520 (1979).
9. J. M. Floryan and W. S. Saric, AIAA J., 10, No. 3, 316-324 (1982).
10. V. V. Babenko and N. F. Yurchenko, Hydrodynamic Questions of Bionics [in Russian], Kiev (1983), pp. 37-46.